

---

# The role of retinal waves and synaptic normalization in retinogeniculate development

---

Stephen J. Eglon†

*School of Cognitive and Computing Sciences, University of Sussex, Brighton BN1 9QH, UK*

The prenatal development of the cat retinogeniculate pathway is thought to involve activity-dependent mechanisms driven by spontaneous waves of retinal activity. The role of these waves upon the segregation of the dorsal lateral geniculate nucleus (LGN) into two eye-specific layers and the development of retinotopic mappings have previously been investigated in a computer model. Using this model, we examine three aspects of retinogeniculate development. First, the mapping of visual space across the whole network into projection columns is shown to be similar to the mapping found in the cat. Second, the simplicity of the model allows us to explore how different forms of synaptic normalization affect development. In comparison to most previous models of ocular dominance, we find that subtractive postsynaptic normalization is redundant and divisive presynaptic normalization is sufficient for normal development. Third, the model predicts that the more often one eye generates waves relative to the other eye, the more LGN units will monocularly respond to the more active eye. In the limit when one eye does not generate any waves, that eye totally disconnects from the LGN allowing the non-deprived eye to innervate all of the LGN. Thus, as well as accounting for normal retinogeniculate development, the model also predicts development under abnormal conditions which can be experimentally tested.

**Keywords:** retinogeniculate development; retinal waves; synaptic normalization; projection columns

## 1. INTRODUCTION

The prenatal development of connections between the retina and the dorsal lateral geniculate nucleus (LGN) in the cat depends on both activity-independent and activity-dependent processes (Goodman & Shatz 1993). Retinal axons from both eyes, guided by molecular cues (Cheng *et al.* 1995), initially make diffuse contacts throughout the LGN (Shatz 1983). By the time of birth, these axons have segregated into two eye-specific layers, with retinotopic mappings of visual space in each layer (figure 1). This refinement of connections is activity-dependent, since activity blockade prevents the eye-specific segregation (Shatz & Stryker 1998). During this period, before the onset of vision, neighbouring retinal cells are spontaneously active, producing waves of activity that travel across the retina (Galli-Resta & Maffei 1988; Maffei & Galli-Resta 1990; Meister *et al.* 1991). This discovery has led to the hypothesis that correlated spontaneous activity refines both the retinotopic mappings and eye-specific segregation in the LGN (Maffei & Galli-Resta 1990; Wong *et al.* 1993).

This hypothesis was first investigated using computer simulation by Keesing *et al.* (1992). They showed that a retinotopic map and eye-specific segregation can develop in a two-layer neural network using local adaptation rules. Although there are many other models of visual pathway development (for review, see Swindale 1996), the postsynaptic sheet in these models is normally of the same or

lower dimensionality than the presynaptic sheet. In contrast, there is a dimensionality expansion in the retinogeniculate pathway: each two-dimensional retinal sheet innervates a three-dimensional LGN. Only one other model has included the same expansion in geometry (Lee & Malpeli 1994). However, this model did not consider the role of activity in shaping receptive fields.

Despite the difference in geometries, previous activity-based models have shown how neural activity guides map formation and ocular dominance (Swindale 1996). For example, the neural activity model (Willshaw & von der Malsburg 1976), produced before retinal waves were discovered, assumed that neighbouring presynaptic units were co-active to produce local within-eye correlations. This model showed that increasing the strength of connections between correlated pre- and postsynaptic units, along with lateral excitation and inhibition among postsynaptic units, was sufficient to produce a retinotopic map of visual space.

Activity-based models of ocular dominance have mostly investigated the formation of interdigitated maps (stripes) in visual cortex (Miller *et al.* 1989; Goodhill 1992; Bauer *et al.* 1997). In these models, the between-eye correlations affect ocularity segregation in two ways. First, small, positive between-eye correlations inhibit development of monocular units in models using correlational learning rules (Dayan & Goodhill 1992). Second, stripe width decreases as between-eye correlations increase (Goodhill 1992). However, retinal waves are generated independently in each eye, so positive between-eye correlations should be absent during retinogeniculate development.

†Present address: Centre for Cognitive Science, University of Edinburgh, Edinburgh EH8 9LW, UK (stephen@anc.ed.ac.uk).

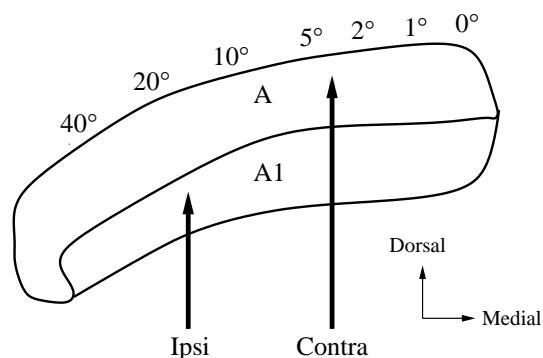


Figure 1. Organization of retinal inputs in the mature cat LGN (coronal section). Retinal inputs segregate into two layers: contralateral axons to layer A and ipsilateral axons to layer A1. Visual azimuth (shown in degrees) varies smoothly across the medio-lateral dimension of the LGN. All LGN cells within a vertical column respond to the same region of visual space. Visual elevation (not shown) maps along the anterior–posterior dimension.

Table 1. *Simulation parameters*

term	meaning	value
$p_w$	probability of a new wave starting	0.02
$\sigma_w$	width of the Gaussian for waves	1.00
$R$	refractory period between waves	1
$W$	duration of wave	50
$X_{\text{pre}}$	number of units in each retina	50
$N_{\text{pre}}$	number of presynaptic units	100
$X_{\text{post}}$	number of units in LGN row	10
$Y_{\text{post}}$	number of units in LGN column	8
$N_{\text{post}}$	number of postsynaptic units	80
$T_{\text{pre}}$	presynaptic normalization target	1.0
$T_{\text{post}}$	postsynaptic normalization target	1.25 <sup>a</sup>
$r_s$	rate of subtractive normalization	1.0
$\alpha$	presynaptic activity threshold	0.1
$\beta$	postsynaptic activity threshold	0.0125
$\epsilon$	correlational rule constant	0.01
$p_g$	probability of using growth rule	0.01
$\gamma_g$	growth rule constant	0.1
$r_g$	size of growth rule	[2, 1, 0]
$t_g$	growth rule decay time	200

<sup>a</sup>  $T_{\text{pre}}$  and  $T_{\text{post}}$  are related by  $N_{\text{pre}} \times T_{\text{pre}} = N_{\text{post}} \times T_{\text{post}}$ , since the total weight strength in the network must be the same using either pre- or postsynaptic normalization.

In this paper we first replicate the main results of the Keesing model, showing how eye-specific layers and retinotopic mappings form within the LGN. Second, we systematically explore the role of the different forms of normalization in the model to discover if both pre- and postsynaptic normalization are necessary. Third, we simulate monocular deprivation conditions by changing the relative rates of retinal wave generation.

## 2. METHODS

In this section we summarize the model presented by Keesing *et al.* (1992). Some details of the model that we present here were omitted from the original publication. We also describe the methods used for analysing network development. All model parameters are listed in table 1.

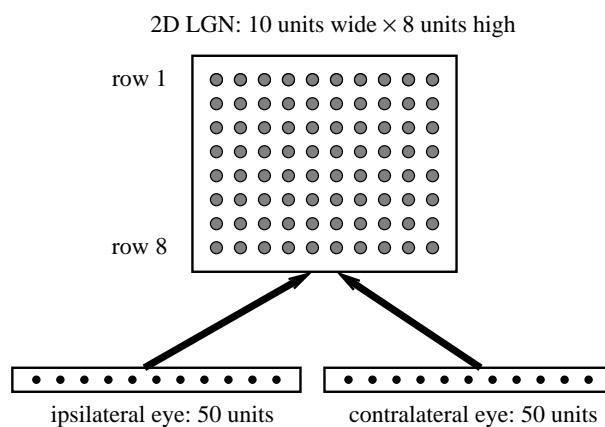


Figure 2. Network architecture. Ipsilateral units (left eye) are indexed  $i = 1 \dots 50$  and contralateral units (right eye)  $i = 51 \dots 100$ . LGN units are numbered row-by-row, with unit 1 in the top left corner, and unit 80 in the bottom right corner.

### (a) Architecture

The model represents two one-dimensional retinæ inner-venating a two-dimensional coronal slice of a binocular region of the left LGN (figure 2). Each retina represents a group of cells that will eventually sample a region of the visual field of fixed elevation and varying azimuth. Units at the same position within each retina sample the same region of the visual field. Each retinal unit  $i$  connects to each LGN unit  $j$  by an adjustable weight  $w_{ij}$ . Inputs to the LGN from inhibitory interneurons and corticogeniculate axons are ignored since they are both immature during prenatal development relative to retinogeniculate inputs (Shatz & Kirkwood 1984; Weber & Kalil 1987). The dimensionality of the retinæ and LGN were reduced to keep the simulation fairly small. Also, the C layers of the LGN are ignored for simplicity.

### (b) Initial weights

The initial weights incorporate two biases reflecting the state of the retinogeniculate pathway initially set up by activity-independent mechanisms. First, an ocularity bias reflects the earlier arrival of contralateral axons into the LGN (Shatz 1983). This is implemented by setting weights from the ipsilateral eye to units in rows seven and eight, and weights from the contralateral eye to units in rows five to eight, of the LGN to random values between 0 and 0.02. All other weights are set to zero. Second, a retinotopic bias ensures that the left end of each retina connects to the left side of the LGN. This bias sets 20% of the weights from the contralateral eye to each LGN unit in row five (or row seven for the ipsilateral eye) to zero (Willshaw & von der Malsburg 1979). Figure 4a shows an example set of initial weights.

### (c) Neural activity

Retinal waves are independently generated in each eye. Both eyes are initially silent. At each time-step, if no wave is present, a new wave is initiated with probability  $p_w$ . A wave starts at either the left- or right-hand side of the retina, and moves one unit per time-step to the other side. Once the wave reaches the other side of the retina, it goes into a refractory period for  $R$  time-steps, after which a new wave may then be initiated. The wave is simply modelled as a Gaussian function of position (of standard deviation  $\sigma_w$ ) from the wavefront.

The activity of each LGN unit,  $y_j$ , is a linear sum of the activity of each retinal unit  $x_i$  modulated by the weight strength between

units:  $y_j = \sum_{i=1}^{N_{\text{pre}}} w_{ij} x_i$ . No non-linearities were required in this activation function, although the correlational rule (see below) includes a term,  $\beta$ , which acts as a threshold for LGN activity.

#### (d) *Weight adaptation mechanisms*

Weights are updated using four rules. Each rule produces a weight change  $\Delta w_{ij}$  for each weight that is added to  $w_{ij}$  to make a new value.

##### (i) *Correlational rule*

$$\Delta w_{ij} = \epsilon(x_i - \alpha)(y_j - \beta),$$

where  $\alpha$ ,  $\beta$  and  $\epsilon$  are constants. This rule captures the Hebbian principle that if the activity of pre- and postsynaptic units is correlated, the strength of the connection between the units should be increased.

##### (ii) *Normalization*

$$\Delta w_{ij} = w_{ij} \left( \frac{T_{\text{pre}}}{\sum_{k=1}^{N_{\text{post}}} w_{ik}} - 1 \right) \quad (\text{divisive presynaptic}),$$

$$\Delta w_{ij} = \frac{T_{\text{post}}}{N_{\text{pre}}} \left( T_{\text{post}} - \sum_{k=1}^{N_{\text{pre}}} w_{kj} \right) \quad (\text{subtractive postsynaptic}).$$

Weight normalization implements the natural constraint that synaptic strengths have an upper limit. These rules fix the sum of weights for each pre- or postsynaptic unit at  $T_{\text{pre}}$  or  $T_{\text{post}}$ .

##### (iii) *Growth rule*

$$\Delta w_{ij} = \gamma_g \sum_{k \in \text{neigh}(j)} w_{ik}.$$

This rule mimics the branching of retinal axons into neighbouring LGN neurons. The set  $\text{neigh}(j)$  contains the index number of LGN units within a square of side-length  $(2r_g + 1)$  centred on unit  $j$ . To avoid border effects, units at the left and right edges of the LGN are considered adjacent using wrap-around.

##### (iv) *Weight bounds*

$$w_{ij} \geq 0.$$

Each weight represents an excitatory connection, and must therefore be non-negative to prevent it exerting an inhibitory effect. Unless stated otherwise, no upper bound is placed on individual weights.

One iteration of the model corresponds to updating the position of any retinal waves or possibly generating new waves, calculating LGN activity and updating weights using the correlational rule. One epoch of the model corresponds to 100 iterations. After each epoch, presynaptic normalization is applied first followed by postsynaptic normalization. The growth rule is used probabilistically after each iteration with a small fixed probability  $p_g$ . The neighbourhood size,  $r_g$ , decreases by one unit every  $t_g$  epochs until it reaches zero, when the growth rule is no longer used.

#### (e) *Measures of development*

Two quantitative measures summarize development. First, the relative strength of inputs from each eye to every postsynaptic unit is shown in an ocularity plot. Each postsynaptic unit is represented by a box within the plot. The monocularity index of a unit,  $z_j$ , determines the size and colour of the box:

$$z_j = \frac{t_j^{\text{left}}}{t_j^{\text{left}} + t_j^{\text{right}}} - \frac{1}{2},$$

where

$$t_j^{\text{left}} = \sum_{i=1}^{X_{\text{pre}}} w_{ij} \quad \text{and} \quad t_j^{\text{right}} = \sum_{i=X_{\text{pre}}+1}^{2X_{\text{pre}}} w_{ij}.$$

Boxes are coloured white if the left eye is dominant ( $z_j > 0$ ) and black if the right eye is dominant ( $z_j < 0$ ). Box size is proportional to the magnitude of  $z_j$ . Any unit whose sum of weights is less than 0.005 is considered dead and is represented by a grey circle to show it receives no retinal input. Second, to monitor retinotopic development, we measure the receptive field centre,  $\bar{x}_j$ , and the receptive field width,  $s_j$ , of the dominant eye's weights for each postsynaptic unit:

$$\bar{x}_j = \frac{1}{m_j} \sum_{i=1}^{X_{\text{pre}}} i w'_{ij} \quad s_j = \left( \frac{1}{m_j} \sum_{i=1}^{X_{\text{pre}}} ((i - \bar{x}_j)^2 w'_{ij}) \right)^{0.5},$$

where

$$m_j = \sum_{i=1}^{X_{\text{pre}}} w'_{ij} \quad \text{and} \quad w'_{ij} = \begin{cases} w_{ij} & \text{if } z_j \geq 0 \\ w_{(i+X_{\text{pre}})j} & \text{if } z_j < 0 \end{cases}.$$

The receptive field width and centre are plotted for all units as error bars in a receptive field plot ( $x$ -axis shows receptive field centre;  $y$ -axis shows postsynaptic unit number). The error bar line-style (solid or dashed) indicates the dominant eye of each unit. This measure assumes the postsynaptic weight vector is unimodal, which is reasonable during the later stages of development (figure 3).

### 3. RESULTS

The results are divided into three sections. First, we show how retinotopy and ocular segregation develop under normal conditions. Second, we investigate the roles of the two different normalization schemes in the model. Third, we explore the effect of modifying the rate of wave generation on network development.

#### (a) *Development of retinotopy and ocular segregation*

First, we examine the refinement of retinal connections to one LGN unit (figure 3). The unit starts with a broad binocular receptive field. In the early stages of development, the weight vector smoothes out and then gradually narrows and becomes strongly responsive to the ipsilateral eye. The unit eventually receives almost all its input from a few neighbouring ipsilateral units.

Figure 4 shows typical ocularity and retinotopy development in the network. Since contralateral inputs are initially higher within the LGN, the growth rule pushes them to the top of the LGN first. As they reach the top, they lose their contacts in the bottom half of the network because each retinal unit is forced to make a limited number of contacts. This allows ipsilateral inputs to dominate in the bottom half of the network, dividing the LGN into two equal-sized monocular layers. Retinotopic refinement begins with the growth rule copying the initial retinotopic bias from one row of LGN units to all other rows. Most LGN units initially receive diffuse inputs from many retinal units, indicated by the large receptive field widths. The receptive fields gradually narrow, with the

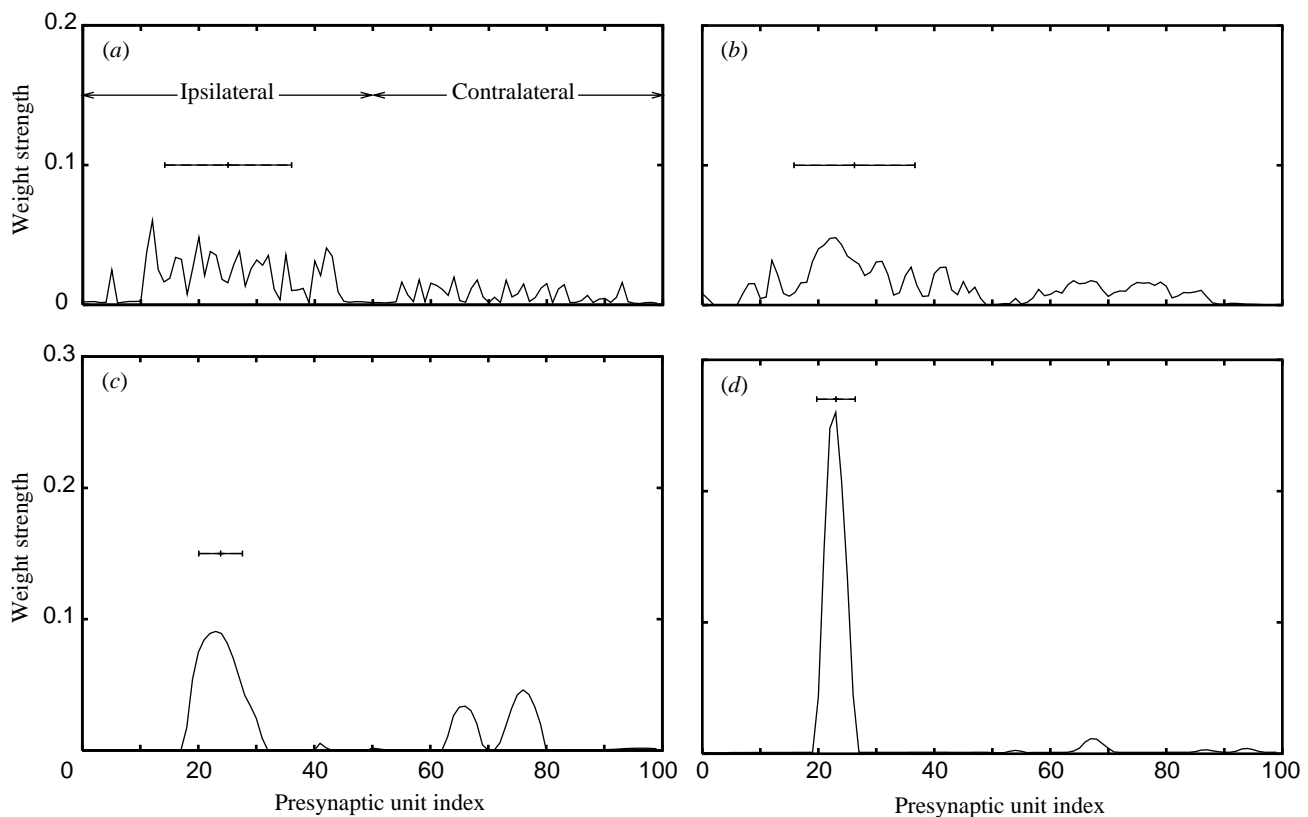


Figure 3. Receptive field refinement for one postsynaptic unit. Each plot shows the strength of connections to one postsynaptic unit. The error bar shows the receptive field centre and width of the weight vector for the dominant eye. (a) Epoch 10. (b) Epoch 100. (c) Epoch 300. (d) Epoch 1500.

receptive field centre varying smoothly across a row of LGN units.

Ocular segregation is robust to changes in initial weights, providing contralateral inputs always start in a higher row of the LGN than ipsilateral inputs. Reducing the initial retinotopic bias below 20% of weights usually prevented the development of global topographic order, with several discontinuities in the receptive field centre of neighbouring units.

One description missing from the original paper was how visual space maps onto the whole LGN—only the mapping into one row of LGN units was considered. Figure 5 shows an example set of projection columns formed within the network. All units within each LGN column have similar receptive field centres, even across the boundary between layer A and A1. Table 2 quantifies this mapping, showing the mean receptive field position smoothly increasing across LGN columns.

### (b) Role of normalization

Weight normalization is used to keep weights bounded and to introduce competition for limited resources. A common method, as used here, is to keep the sum of a unit's weights fixed by either dividing or subtracting a constant from each weight. These two methods, called divisive and subtractive normalization, have different effects on the weight vector. Divisive normalization produces graded receptive fields with weights taking on a range of values, whereas subtractive normalization pushes weights to extreme values, producing much narrower and sharper receptive fields (Miller & Mackay 1994; Goodhill & Barrow 1994).

To ensure all weights in a network remain bounded, it is sufficient to normalize either the weights from each presynaptic unit or the weights to each postsynaptic unit. Biological evidence supports both forms of normalization in different systems (Hayes & Meyer 1988; Norden & Constantine-Paton 1994). It is common, however, to use both pre- and postsynaptic normalization to force either graded or sharp receptive fields to develop, and to ensure all pre- and postsynaptic units stay connected in the network (Miller *et al.* 1989; Keesing *et al.* 1992; Goodhill 1992). Although in principle it is not possible to satisfy both pre- and postsynaptic normalization (applying the second constraint breaks the first), in practice, simulations show that both forms can be satisfied (Goodhill 1992; Eglén 1997).

To investigate the relative importance of pre- and postsynaptic normalization, we systematically examined the effects of using nine different combinations of normalization: for each set of units (pre- and postsynaptic) we can normalize weights subtractively, divisively or not at all. (There are another four cases if postsynaptic units are normalized before presynaptic units. However, normalizing postsynaptic units first removes any initial ocularity bias and so these cases are ignored.)

Networks using divisive presynaptic normalization develop normal retinotopic maps, regardless of the form of postsynaptic normalization (left column of figure 6). Projection columns form because the weight strength available to each retinal unit is shared among units in adjacent rows of the LGN (figure 8*a*). In contrast, subtractive presynaptic normalization (middle column of figure 6) produces much narrower receptive fields than

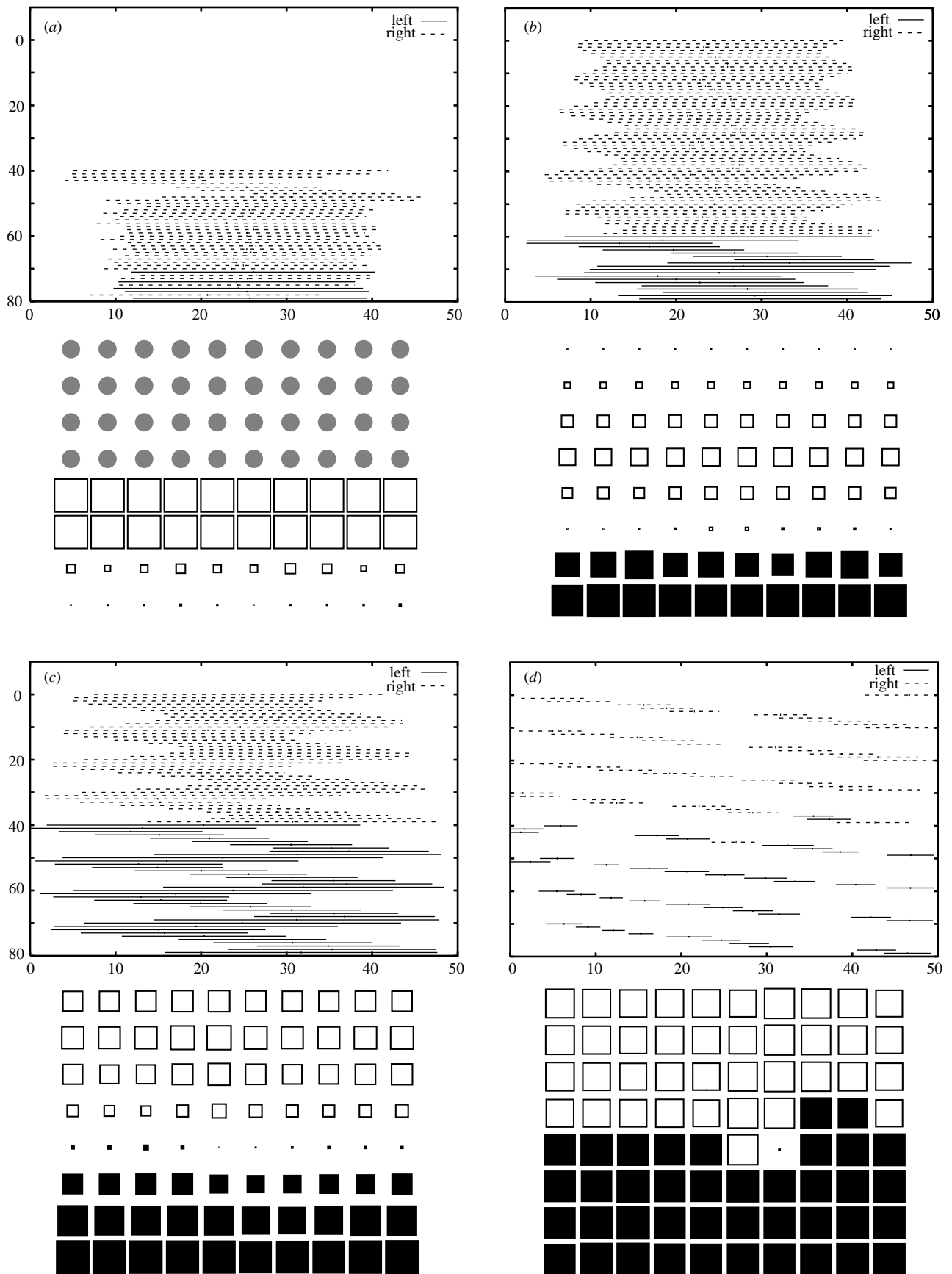


Figure 4. Normal development of retinotopy and eye-specific segregation. (a-d) Receptive field plot (top) and ocularity plot (bottom). (a) Initial state. (b) Epoch 40. (c) Epoch 100. (d) Epoch 1500.

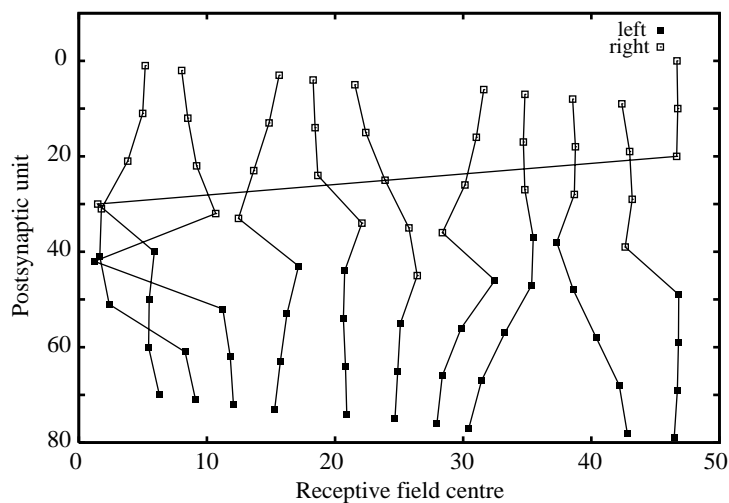


Figure 5. Final projection columns for network in figure 4*d*. The receptive field centre of each postsynaptic unit is plotted as a square, colour coded to indicate the dominant eye. Lines are drawn between nearest neighbouring units in each LGN column. Units in column one respond to both left and right ends of the retina in this network due to wrap-around.

Table 2. Mean receptive field centre of units within each LGN column (normal development)

(Means computed from network shown in figure 5.)

column	1	2	3	4	5	6	7	8	9	10
mean	20.6 <sup>a</sup>	4.7	9.1	15.1	20.1	24.3	30.0	33.8	35.2	44.8
s.d.	20.3	2.7	3.3	1.4	1.3	1.6	1.6	1.8	3.1	2.0

<sup>a</sup> High value caused by wrap-around (see figure 5).

divisive normalization (table 3). However, the overall retinotopic order is lost within both rows and columns of the LGN because presynaptic subtractive normalization produces sharp projective fields to just one row, rather than several rows, of the LGN (figure 8*b*). Finally, in the absence of presynaptic normalization (right column of figure 6), the growth rule drives most of the weight strength for each postsynaptic unit to a small group of presynaptic units, with the remaining presynaptic units losing contact in the LGN. The case when there is no normalization at all (bottom right of figure 6) is presented for completeness; in this condition, many weights become very large.

The segregation into two monocular layers is more robust and occurs if there is some form of presynaptic normalization (figure 7*a*), although if it is subtractive, many units lose all retinal input (figure 7*b*). However, in the absence of presynaptic normalization, only a small number of contralateral units remain connected to the LGN; the remaining retinal units from both eyes lose all contact (figure 7*c*).

Subtractive presynaptic normalization can be coerced into sharing its weight resource among different LGN units by imposing a maximum value (or cap) on individual weights. For example, when each weight is constrained to be no larger than 0.2, each retinal unit contacts multiple LGN units within a column (figure 8*c*). However, unlike divisive presynaptic normalization, map formation is highly sensitive to the values of the cap and the enforcement rate of subtractive normalization.

### (c) Monocular deprivation

It is reasonable to assume that waves in the two eyes of an animal have similar spatio-temporal properties since

they are independently generated within each eye. Changing the relative rate of wave generation between eyes, either by monocular enucleation or intraocular activity blockade, causes the non-deprived eye to invade areas of the LGN that usually receive inputs from the other eye (Guillery *et al.* 1985; Penn *et al.* 1998). Monocular enucleation also produces novel laminations of the remaining eye's inputs: the cat LGN forms a magnocellular and parvocellular layer (Garraghty *et al.* 1988), whereas the ferret LGN forms on- and off-centre layers (Morgan & Thompson 1993). The effect of monocular enucleation upon retinotopic development has so far not been reported.

To investigate if the model accounts for these deprivation results, the rate of wave generation,  $p_w$ , for the right eye was fixed at 0.02, while the rate for the left eye was 0–0.02. The overall probability of activity in an eye,  $O$ , is given by:

$$O = \frac{W}{((1 - p_w)/p_w) + R + W},$$

where  $(1 - p_w)/p_w$  is the average time between one wave finishing and the next starting. Values of  $p_w$  were chosen in a set of experiments such that a wide range of values for  $O$  were sampled.

Two small changes to the model were needed for these experiments. First, when waves are not generated very often ( $p_w < 0.005$ ), the activity of pre- and postsynaptic units will mostly be below the thresholds ( $\alpha$ ,  $\beta$ ) of the correlational rule. This causes the rule to non-selectively increase most connections, inhibiting both ocular and retinotopic refinement. To prevent this, we ignore weight changes from the correlational rule when both pre- and postsynaptic activity is below threshold. Second, the

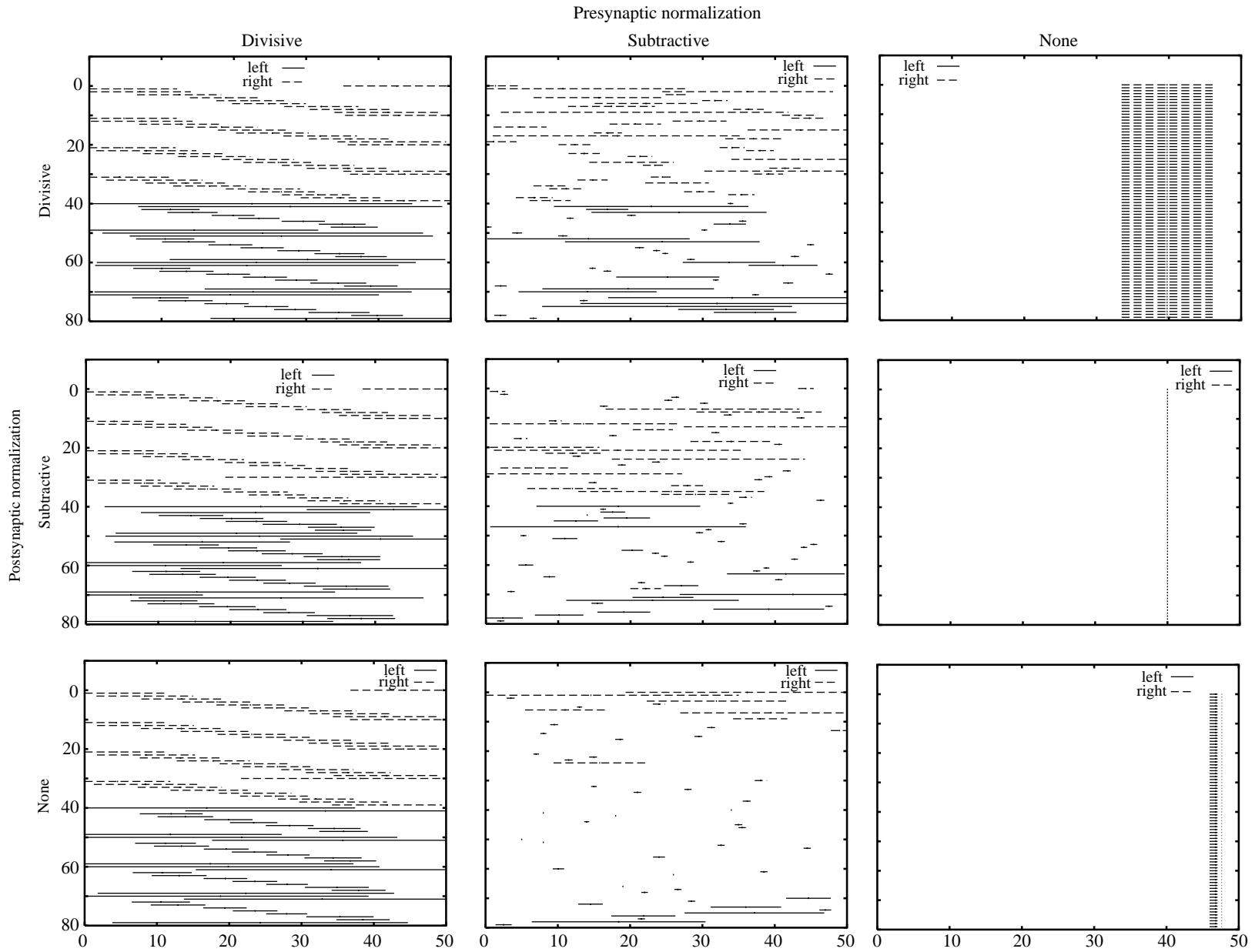


Figure 6. Final receptive field plots for the nine different combinations of pre- and postsynaptic normalization.

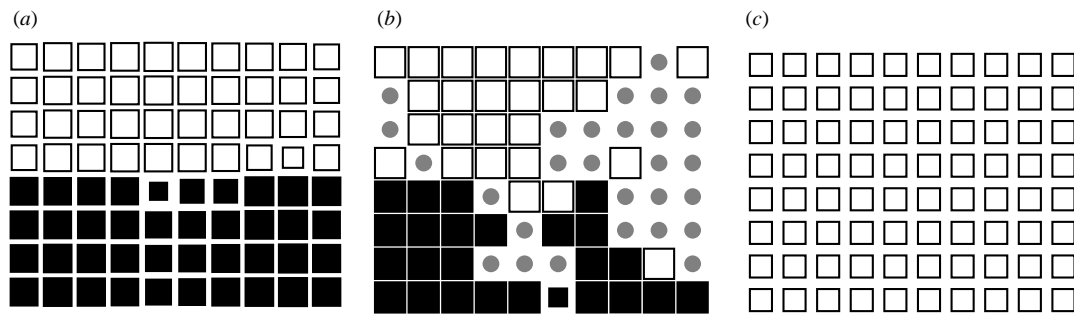


Figure 7. Final ocularity plots under different normalization conditions. (a) Divisive presynaptic normalization and subtractive postsynaptic normalization. (b) Subtractive presynaptic normalization only. (c) Divisive postsynaptic normalization only.

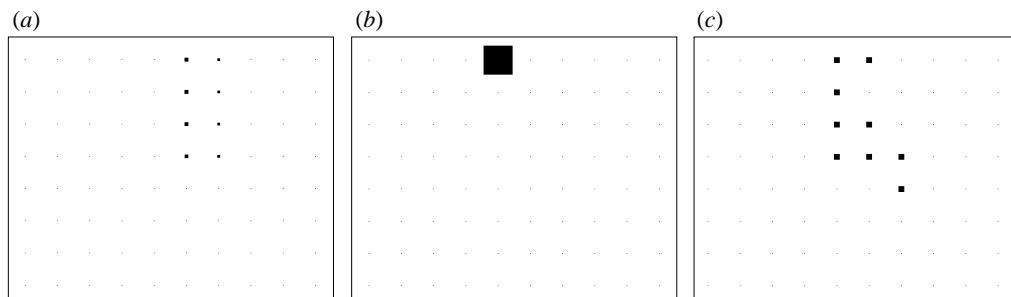


Figure 8. Projective field plots under different presynaptic normalization conditions (no postsynaptic normalization). Each plot shows the strength of connections from a central contralateral unit to the LGN. Box size is proportional to the connection strength from the retinal unit to each LGN unit. All plots drawn to the same scale (maximum value 1.0). The smallest dots in each plot represent weights of zero magnitude and are drawn just to show the position of each LGN unit. (a) Divisive normalization. (b) Subtractive normalization. (c) Capped subtractive normalization. All weights are pushed to extreme values (0.0 or 0.2). (The sum of weights in this case, 1.8, is bigger than the target value  $T_{\text{pre}}$ , 1.0, since  $r_s = 0.05$  here.)

Table 3. *Final median receptive field width under different normalization conditions*

	presynaptic normalization		
	divisive	subtractive	none
postsynaptic normalization			
divisive	5.07	2.24	6.30
subtractive	4.78	0.83	0.00 <sup>a</sup>
none	5.00	0.57 <sup>b</sup>	0.86

<sup>a</sup> In this condition each LGN unit had only one non-zero weight and so each receptive field width was zero.

<sup>b</sup> Medians measured over 80 LGN units, except for this condition when 28 dead units were excluded.

normalization was weakened by ignoring positive values of  $\Delta w_{ij}$  from the presynaptic normalization rule. In the limit when an eye is not generating any retinal waves, this allows the inactive retinal units to lose all contact with the LGN.

Figure 9 and table 4 summarize the monocular deprivation experiments. The more often waves are present in the right eye relative to the left, the more LGN units become responsive to the right eye. This occurs by recruiting extra LGN units at the border between the two monocular layers. In the limit when no waves are generated in the left eye, all LGN units are either monocularly responsive to the right eye or dead. Similar results were achieved when depriving the right eye, indicating these results are independent of the initial ocularity bias.

Table 4. *Mean number of LGN units monocularly responsive to each eye for different rates of wave generation*

( $p_w$  for the right eye was fixed at 0.020, whilst  $p_w$  for the left eye was varied. Mean and standard deviation for each value of  $p_w$  calculated over unit counts from 20 simulations with different initial weights.)

$p_w$	$O$	mean number of units $\pm$ s.d.		
		left	right	dead
0.020	0.50	39.3 $\pm$ 0.9	40.0 $\pm$ 0.4	0.8 $\pm$ 0.9
0.010	0.33	32.7 $\pm$ 1.2	46.3 $\pm$ 1.3	1.1 $\pm$ 0.8
0.005	0.20	23.2 $\pm$ 1.9	54.0 $\pm$ 2.2	2.9 $\pm$ 1.8
0.0035	0.15	12.4 $\pm$ 2.3	61.2 $\pm$ 2.0	6.5 $\pm$ 2.1
0.002	0.01	3.2 $\pm$ 2.0	68.0 $\pm$ 2.7	8.9 $\pm$ 2.3
0.000	0.00	0.1 $\pm$ 0.2	73.4 $\pm$ 0.0	6.6 $\pm$ 2.5

Monocular deprivation also tends to make projection columns wider than those produced under normal conditions (compare figure 9e with figure 5). The mapping of visual space is still retinotopic, however, with the mean receptive field centre increasing smoothly across successive LGN columns (table 5).

#### 4. DISCUSSION

This paper makes three main contributions. First, we have replicated the results presented by Keesing *et al.* (1992), showing how both ocular segregation and retinotopic

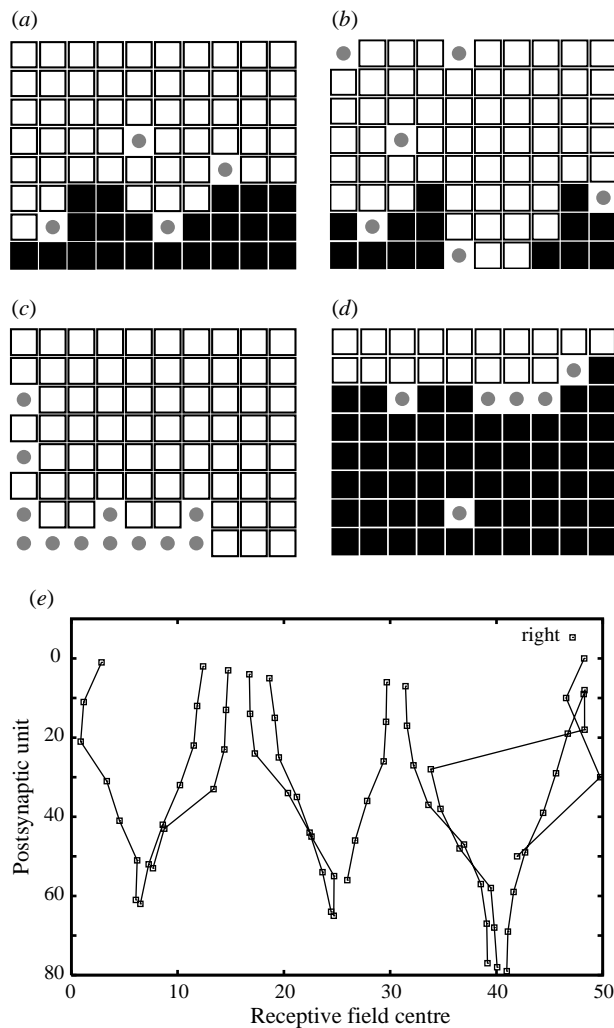


Figure 9. Effect of reducing the probability of wave generation,  $p_w$ , for one eye whilst  $p_w$  fixed at 0.02 for other eye. (a–c) Left eye deprived. (a)  $p_w = 0.005$ . (b)  $p_w = 0.0035$ . (c)  $p_w = 0.002$ . (d) Right eye deprived.  $p_w = 0.0035$ . (e) Projection column plot (same format as figure 5) corresponding to ocularity plot in (c); no units respond to the left eye.

mappings arise from a combination of local activity-dependent rules and broad assumptions on the initial connectivity. We have also shown that each row of the LGN contains a complete map of visual space and these maps are aligned across LGN rows into projection columns, similar to those found in the cat (Sanderson 1971).

Second, we have shown that the model requires only presynaptic normalization of synaptic connections, and that retinotopic development, although not eye-specific segregation, depends on this normalization being enforced divisively. The finding that postsynaptic normalization is redundant in the model is surprising, given its

necessity in previous models (Miller *et al.* 1989; Goodhill 1992). Another recent model has also shown that subtractive postsynaptic normalization is not necessary, although this may be a consequence of the size of the input stimuli used (Bauer *et al.* 1997). Hence, postsynaptic normalization may not be required here because of the local nature of the within-eye correlations and the absence of between-eye correlations. This model also verifies that whereas divisive normalization produces graded receptive fields, subtractive normalization creates much sharper receptive fields (Miller & Mackay 1994; Goodhill & Barrow 1994). Subtractive normalization can produce broader fields only by capping individual weights at some carefully chosen maximum value.

Third, the model predicts that the size of each monocular layer depends on the relative rate of retinal wave generation. This prediction could be experimentally tested by long-term intraocular application of cholinergic enhancers that increase wave frequency, such as neostigmine (Feller *et al.* 1996; Sernagor & O'Donovan 1997). Although other geniculocortical models show similar results (von der Malsburg 1979; Goodhill & Willshaw 1994), this model also shows that when an eye never generates waves, it totally disconnects from the LGN (Penn *et al.* 1998).

This simple model can be extended in several ways. First, the model could use two-dimensional (2D) retina and a three-dimensional LGN. As well as allowing us to check that the current results are not an artefact of the reduction in dimensionality, the waves will be able to travel in many different directions across 2D retina. The waves themselves can also be made more realistic by using a recent model of wave generation and propagation (Feller *et al.* 1997). The model could also be used to investigate the activity-dependent development of on- and off-centre sublayers within each monocular layer (Stryker & Zahs 1983; Hahm *et al.* 1991). Preliminary results from the current model (Eglén 1997) show that on- and off-centre retinal inputs segregate only when using unrealistic on-off cell anticorrelations (Wong & Oakley 1996). For this task, competitive learning rules may produce better results than the correlational rule used here.

We have demonstrated that a combination of activity-independent and activity-dependent mechanisms can produce a highly ordered set of retinogeniculate connections. In this model, the adjustment of connection strengths plays a central role in development. An alternative recently proposed for primate LGN is that selective loss of inappropriately projecting retinal cells may drive LGN segregation (Snider *et al.* 1997). Future models could investigate the relative importance of refining connections and cell death in forming the mature pattern of connectivity between the retina and LGN.

Table 5. Mean receptive field centre of units within each LGN column after monocular deprivation

(Data taken from network shown in figure 9e;  $n$  is the number of non-dead units.)

column	1	2	3	4	5	6	7	8	9	10
mean	46.6	3.6	9.8	12.3	20.2	21.5	28.2	35.3	40.1	43.9
s.d.	2.9	2.0	2.2	2.9	3.1	2.4	1.5	3.2	5.2	2.6
$n$	4	7	7	6	7	7	6	8	8	8

I thank Harry Barrow for supervising my PhD thesis, from where this work originates. Thanks also to Julian Budd and David Willshaw for critical reading of this manuscript. This work was funded by a PhD scholarship from the University of Sussex and a Mathematical Biology Fellowship from the Wellcome Trust.

## REFERENCES

- Bauer, H.-U., Brockmann, D. & Geisel, T. 1997 Analysis of ocular dominance pattern formation in a high-dimensional self-organizing-map model. *Network: Comput. Neural Syst.* **8**, 17–33.
- Cheng, H.-J., Nakamoto, M., Bergemann, A. D. & Flanagan, J. G. 1995 Complementary gradients in expression and binding of ELF-1 and Mek4 in development of the topographic retinotectal projection map. *Cell* **82**, 371–381.
- Dayan, P. S. & Goodhill, G. J. 1992 Perturbing Hebbian rules. In *Advances in neural information processing systems*, vol. 4 (ed. J. E. Moody, S. J. Hanson & R. P. Lippmann), pp. 19–26. San Mateo: Morgan Kaufmann.
- Eglén, S. J. 1997 Modelling the development of the retinogeniculate pathway. PhD thesis, School of Cognitive and Computing Sciences, Sussex University, UK.
- Feller, M. B., Wellis, D. P., Stellwagen, D., Weblin, F. S. & Shatz, C. J. 1996 Requirement for cholinergic synaptic transmission in the propagation of spontaneous retinal waves. *Science* **272**, 1182–1187.
- Feller, M. B., Butts, D. A., Aaron, H. L., Rokhsar, D. S. & Shatz, C. J. 1997 Dynamic processes shape spatiotemporal properties of retinal waves. *Neuron* **19**, 293–306.
- Galli-Resta, L. & Maffei, L. 1988 Spontaneous impulse activity of rat retinal ganglion cells in prenatal life. *Science* **242**, 90–91.
- Garraghty, P. E., Shatz, C. J. & Sur, M. 1988 Prenatal disruption of binocular interactions creates novel lamination in the cat's lateral geniculate nucleus. *Vis. Neurosci.* **1**, 93–102.
- Goodhill, G. J. 1992 Correlations, competition and optimality: modelling the development of topography and ocular dominance. PhD thesis, School of Cognitive and Computing Sciences, Sussex University, UK.
- Goodhill, G. J. & Barrow, H. G. 1994 The role of weight normalization in competitive learning. *Neural Comp.* **6**, 255–269.
- Goodhill, G. J. & Willshaw, D. J. 1994 Elastic net model of ocular dominance—overall stripe pattern and monocular deprivation. *Neural Comp.* **6**, 615–621.
- Goodman, C. S. & Shatz, C. J. 1993 Developmental mechanisms that generate precise patterns of neuronal connectivity. *Cell* **72**, 77–98.
- Guillery, R. W., Lamantia, A. S., Robson, J. A. & Huang, K. 1985 The influence of retinal afferents upon the development of layers in the dorsal lateral geniculate-nucleus of mustelids. *J. Neurosci.* **5**, 1370–1379.
- Hahn, J. O., Langda, R. B. & Sur, M. 1991 Disruption of retinogeniculate afferent segregation by antagonists to NMDA receptors. *Nature* **351**, 568–570.
- Hayes, W. P. & Meyer, R. L. 1988 Retinotopically inappropriate synapses of subnormal density formed by surgically misdirected optic fibers in goldfish tectum. *Dev. Brain Res.* **38**, 304–312.
- Keesing, R., Stork, D. G. & Shatz, C. J. 1992 Retinogeniculate development: the role of competition and correlated retinal activity. In *Advances in neural information processing systems*, vol. 4 (ed. J. E. Moody, S. J. Hanson & R. P. Lippmann), pp. 91–97. San Mateo: Morgan Kaufmann.
- Lee, D. Y. & Malpeli, J. G. 1994 Global form and singularity—modeling the blind spots role in lateral geniculate morphogenesis. *Science* **263**, 1292–1294.
- Maffei, L. & Galli-Resta, L. 1990 Correlation in the discharges of neighbouring rat retinal ganglion cells during prenatal life. *Proc. Natn. Acad. Sci. USA* **87**, 2861–2864.
- Meister, M., Wong, R. O. L., Baylor, D. A. & Shatz, C. J. 1991 Synchronous bursts of action potentials in ganglion cells of the developing mammalian retina. *Science* **252**, 939–943.
- Miller, K. D. & Mackay, D. J. C. 1994 The role of constraints in Hebbian learning. *Neural Comp.* **6**, 100–126.
- Miller, K. D., Keller, J. B. & Stryker, M. P. 1989 Ocular dominance column development—analysis and simulation. *Science* **245**, 605–615.
- Morgan, J. & Thompson, I. D. 1993 The segregation of on-center and off-center responses in the lateral geniculate nucleus of normal and monocularly enucleated ferrets. *Vis. Neurosci.* **10**, 303–311.
- Norden, J. J. & Constantine-Paton, M. 1994 Dynamics of retinotectal synaptogenesis in normal and 3-eyed frogs: evidence for the postsynaptic regulation of synapse number. *J. Comp. Neurol.* **348**, 461–479.
- Penn, A. A., Riquelme, P. A., Feller, M. B. & Shatz, C. J. 1998 Competition in retinogeniculate patterning driven by spontaneous activity. *Science* **279**, 2108–2112.
- Sanderson, K. J. 1971 The projection of the visual field to the lateral geniculate and medial interlaminar nuclei in the cat. *J. Comp. Neurol.* **143**, 101–118.
- Sernagor, E. & O'Donovan, M. J. 1997 Cellular mechanisms underlying retinal waves in the chick embryo. *Soc. Neurosci. Abst.* **23**, 306.
- Shatz, C. J. 1983 The prenatal development of the cat's retinogeniculate pathway. *J. Neurosci.* **3**, 482–499.
- Shatz, C. J. & Kirkwood, P. A. 1984 Prenatal development of functional connections in the cat's retinogeniculate pathway. *J. Neurosci.* **4**, 1378–1397.
- Shatz, C. J. & Stryker, M. P. 1988 Prenatal tetrodotoxin infusion blocks segregation of retinogeniculate afferents. *Science* **242**, 87–89.
- Snider, C. J., Quinto, J. G., Dehay, C., Berland, M., Kennedy, H. & Chalupa, L. M. 1997 Restructuring of retinogeniculate axons plays a minor role in the formation of eye-specific layers in the dLGN of the fetal monkey. *Soc. Neurosci. Abst.* **23**, 1159.
- Stryker, M. P. & Zahs, K. R. 1983 On and off sublaminae in the lateral geniculate nucleus of the ferret. *J. Neurosci.* **3**, 1943–1951.
- Swindale, N. V. 1996 The development of topography in the visual cortex: a review of models. *Network: Comput. Neural Syst.* **7**, 161–247.
- von der Malsburg, C. 1979 Development of ocularity domains and growth behaviour of axon terminals. *Biol. Cybern.* **32**, 49–62.
- Weber, A. J. & Kalil, R. E. 1987 Development of corticogeniculate synapses in the cat. *J. Comp. Neurol.* **264**, 171–192.
- Willshaw, D. J. & von der Malsburg, C. 1976 How patterned neural connections can be set up by self-organization. *Proc. R. Soc. Lond. B* **194**, 431–445.
- Willshaw, D. J. & von der Malsburg, C. 1979 A marker induction mechanism for the establishment of ordered neural mappings: its application to the retinotectal problem. *Phil. Trans. R. Soc. Lond. B* **287**, 203–243.
- Wong, R. O. L. & Oakley, D. M. 1996 Changing patterns of spontaneous bursting activity of on and off retinal ganglion cells during development. *Neuron* **16**, 1087–1095.
- Wong, R. O. L., Meister, M. & Shatz, C. J. 1993 Transient period of correlated bursting activity during development of the mammalian retina. *Neuron* **11**, 923–938.